Photodissociation dynamics of jet-cooled ClNO on S_1(1 $^1A''$): An experimental study

A. Ogai,[a] C. X. W. Qian, and H. Reisler

Department of Chemistry, University of Southern California, Los Angeles, California 90089-0482

We report measurements of photofragment yield (PHOFRY) spectra and NO E, V, R distributions following dissociation of jet-cooled ClNO on the S_1(1 $^1A''$) electronic surface. The dissociative S_1(1 $^1A''$)←S_0(1 $^1A'$) transition shows diffuse vibrational structure with a progression in ν_1, the NO stretch. The absorption and PHOFRY spectra consist of two bands, corresponding to excitations into S_1(000) and S_1(100), whose widths are 1300 ± 100 and 1000 ± 70 cm^{-1}, respectively. The relative partial absorption cross sections are S_1(000):S_1(100) = 2.3:1.0. The narrowing of the absorption bands with increasing ν_1 quanta is a consequence of the mismatch between ν_1 and the free NO vibrational frequency. Dissociations on S_1(000) and S_1(100) yield NO in $v'' = 0$ and 1, respectively. The NO($X^2\Pi$) rotational distributions in $v'' = 0$ and 1 are inverted, peaking at $J'' \sim 30.5$ with widths of 10 ± 1 J'', and they do not vary significantly when the photolysis laser is scanned across the absorption band. The evolution of NO vibrational and rotational excitations appear to be largely uncoupled. In NO $v'' = 0$ and 1, the upper spin–orbit state $^2\Pi_{3/2}$ is more populated than the lower state $^2\Pi_{1/2}$. For both $v'' = 0$ and 1, the Λ-doublet $\Pi(A'')$ component of NO($^2\Pi_{1/2}$) is more populated than the $\Pi(A')$ component by a ratio of $\sim 3:1$, as expected for excitation to a π^* orbital of a'' symmetry, but this propensity is much lower for NO($^2\Pi_{3/2}$), possibly due to perturbations with another surface. The absorption spectra and NO V, R distributions are in good agreement with recent dynamical calculations on a three-dimensional (3-D) potential-energy surface (PES) calculated *ab initio*. The vibrational distribution appears to be determined near the Franck–Condon (FC) region, while final-state interactions affect the rotational distributions at larger Cl–NO separations.

I. INTRODUCTION

The photodissociation dynamics of ClNO has recently attracted considerable experimental and theoretical interest, since several of its dissociative electronic states are easily accessed by tunable dye lasers.[1–8] Thus, the relationship between the electronic structure of the parent molecule and the forces and torques that influence the product state distributions can be studied for several electronic states in the *same* molecule. Fortunately, although some of the electronic absorption bands are broad and overlap other absorption features,[9] the dissociation dynamics seems to evolve on isolated surfaces which are largely uncoupled.[6] In addition, the existence of diffuse vibrational structure in some electronic transitions enables studies of state-specific dissociation dynamics.[6–8]

Early work was hindered by the absence of definitive spectroscopic assignments of the absorption bands, and the spectrum was only recently assigned using a combination of photofragment spectroscopy, vector correlation measurements and *ab initio* calculations.[6] In particular, the lowest absorption feature starting at ~ 620 nm and consisting of a series of diffuse bands is now assigned to the singlet–triplet T_1(1 $^3A''$) transition. It is also proposed that the bands labeled D and C in the original spectrum (i.e., those peaking at ~ 472 and 440 nm[9]) arise from the S_1(1 $^1A''$)←S_0(1 $^1A'$) transition terminating in the (000) and (100) vibrational

levels, respectively, where ν_1 is the NO stretch.[6] The two peaks are separated by the NO stretch frequency, and the experimental measurements show that dissociation in the D band gives rise to NO in $v'' = 0$, while dissociation in the C band yields predominantly NO in $v'' = 1$.[6] The spectroscopic assignments are supported by the measured vector properties and the NO photofragment yield (PHOFRY) spectra.[6] For example, the recoil anisotropy parameters of NO in $v'' = 0$ and 1 monitored with photolysis in the D and C bands, respectively, are similar and typical of a perpendicular $A'' \leftarrow A'$ transition. It is therefore concluded that the S_1(1 $^1A''$)←S_0(1 $^1A'$) transition has a diffuse vibrational structure exhibiting a progression in ν_1.

The *ab initio* potential energy surface (PES) calculated along the reaction coordinate, as well as the available experimental evidence, suggest a fast and direct dissociation on a repulsive surface.[6] With a new 3D PES now available, dynamical calculations become possible, and a data base that can serve to test the theory is highly desirable, especially since previous work in this wavelength region had been done before the correct spectroscopic assignments were available.[4,5] Also, some of the previous work was done with 300-K samples and a single photolysis-probe laser, thereby limiting the tunability of the photolysis wavelength.[4] Work done with expansion-cooled samples addressed mainly the vector properties, and was limited to NO($v'' = 0$).[5]

In this paper, we present additional experimental data on the rotational distributions of NO $v'' = 0$ and 1 produced

---

[a] NSF Predoctoral Fellow.

via S_1 photolysis of expansion-cooled ClNO. In addition, we report measurements of the relative partial absorption cross sections in the D and C bands. These measurements were done by monitoring selected rotational levels in NO $v'' = 0$ and 1 produced via photolysis in the D and C bands, respectively. In a separate publication, Schinke *et al.* compare the experimental results to results of classical and quantal calculations on a 3D PES calculated *ab initio*, and find generally good agreement with the experimental data.[10] Together, the experimental and theoretical efforts yield a fairly complete understanding of the photodissociation dynamics on S_1. In addition, we compare the dissociation dynamics on T_1 and S_1. These two states derive from the same electronic configuration, and the comparison of the dissociation mechanisms provides further insights into the correlation between the electronic structure of the excited state and the forces along the reaction coordinate.

II. EXPERIMENTAL

The experimental arrangement was similar to the one used in our previous studies.[5,6] Briefly, premixed ClNO samples (10/500 Torr in He) were prepared and expanded via a pulsed valve (Lasertechnics, 500-μm diam orifice, $\sim$200-μs pulse duration) into an octagonal fluorescence chamber. The photolysis laser was a Nd:YAG laser pumped dye laser system (Quanta Ray DCR1A/PDL1). The probe laser radiation was obtained from an excimer laser pumped dye laser system (Lambda Physik EMG 101 MSC/FL 2001). The output at 450 nm was frequency doubled with a BBO crystal, and the NO fragments were probed by one-photon laser-induced fluorescence (LIF) via the A $^2\Sigma^+ \leftarrow$ X $^2\Pi$ transition (γ bands) at $\sim$226 nm. The fluorescence was detected by a solar blind photomultiplier tube (PMT) (Hamamatsu R166UH) through an interference filter. The intensity of the probe laser beam was maintained at $< 40 \mu$J in order to avoid saturation, and in particular dissociation of ClNO by the 226-nm radiation.

The two laser beams were collinear and counterpropagating, but perpendicular both to the PMT and to the pulsed valve. The polarization of the photolysis laser was rotated with a half-wave plate, and the desired polarization component was further selected with a Rochon polarizer. In some cases, the polarization was rotated with a pair of prisms. The probe laser was maintained at a vertical polarization. The timing sequence was controlled by a homemade digital delay generator with 20-ns increments, and the delay between the pump and probe lasers was typically 80–160 ns. The observed LIF signals were normalized to both laser intensities. Usually, the signals from 30 to 100 laser firings were averaged for each data point.

ClNO was obtained from Matheson and purified by trap-to-trap distillations. Due to the existence of equilibrium between ClNO and NO, it was impossible to completely eliminate NO contamination. However, since NO produced

in the dissociation was rotationally hot ($J'' > 20.5$), while for the expansion-cooled NO contamination, $J'' < 5.5$, the results reported here were essentially unaffected by NO contamination.

III. RESULTS

The absorption spectrum of 300-K ClNO shows several peaks traditionally assigned by letters.[9] The dissociative $S_1 \leftarrow S_0$ transition $[D_0(\text{ClNO}) = 13\,000\text{ cm}^{-1}]$[11] encompasses the D and C bands peaking at $\sim$472 and 440 nm, respectively.[5,6] NO PHOFRY spectra were obtained by scanning the photolysis laser wavelength while monitoring selected levels of NO($X\,^2\Pi$) 100 ns after dissociation. The PHOFRY spectra obtained when monitoring the $Q_{22}(33.5)$ lines of $v'' = 0$ and 1 are shown in Fig. 1. We find, as before, that when monitoring NO($v'' = 0$) only the D band appears, while when monitoring NO($v'' = 1$) only the C band appears.[6] The peaks are separated by $1500 \pm 100\text{ cm}^{-1}$, corresponding to the NO stretch frequency in S_1, which is similar to the corresponding value in T_1.[8] As discussed before, parent NO stretch excitation evolves adiabatically into NO vibrational excitation, i.e., the C band arises from absorption to S_1 with one quantum of NO stretch excitation.[6] The D and C bands are rather symmetric with widths 1300 ± 100 and $1000 \pm 70\text{ cm}^{-1}$ full width at half-maximum (FWHM), respectively. The relative intensities of the bands shown in Fig. 1 are normalized and reflect the relative partial absorption cross sections. The $Q_{22}(33.5)$ line intensities were converted into relative absorption cross sections in the following way. The $Q_{22}(33.5)$ line intensities in $v'' = 0$ and 1 were recorded at 472 and 440 nm, respectively, since these two photoexcitation wavelengths correspond to maxima in the D and C absorption bands. Usually, many factors have to be accounted for when extracting relative state populations from line intensities and the measured signal intensities depend on: (i) photolysis and probe laser powers; (ii) detection system sensitivities (e.g., PMT and filter responses); (iii) oscillator strengths, FC factors, and line-strength factors for the NO($A\,^2\Sigma^+$) $\leftarrow$ NO($X\,^2\Pi$) absorption; (iv) oscillator strengths, FC factors, and line-strength factors for emissions from the excited A $^2\Sigma^+$ rovibronic level of NO to the spectroscopically allowed ground-state rovibronic levels; and (v) detection biases due to laser polarization and alignment effects. In our measurements, the same rotational line was monitored in both vibrational levels, and the rotational alignment parameters were similar (see below); thus, correction (v) was unnecessary. In addition, we chose an experimental scheme that minimized systematic errors due to detection system response. The excitations of both $v'' = 0$ and $v'' = 1$ terminated in a common NO($A\,^2\Sigma^+$) level, $v' = 0, J' = 33.5$, and therefore, fluorescence from the same level was monitored when detecting NO in $v'' = 0$ and 1. Thus, correction factors due only to (i) and (iii) had to be introduced, yielding

$$\frac{\text{NO}(v''=0)}{\text{NO}(v''=1)} = \frac{[Q_{22}(33.5)]_0 \cdot [S_{22}(33.5)]_1 \cdot \text{FC}(0-1) \cdot I_{\text{ph}}(440) \cdot I_{\text{pr}}(0-1)}{[Q_{22}(33.5)]_1 \cdot [S_{22}(33.5)]_0 \cdot \text{FC}(0-0) \cdot I_{\text{ph}}(472) \cdot I_{\text{pr}}(0-0)}, \tag{1}$$
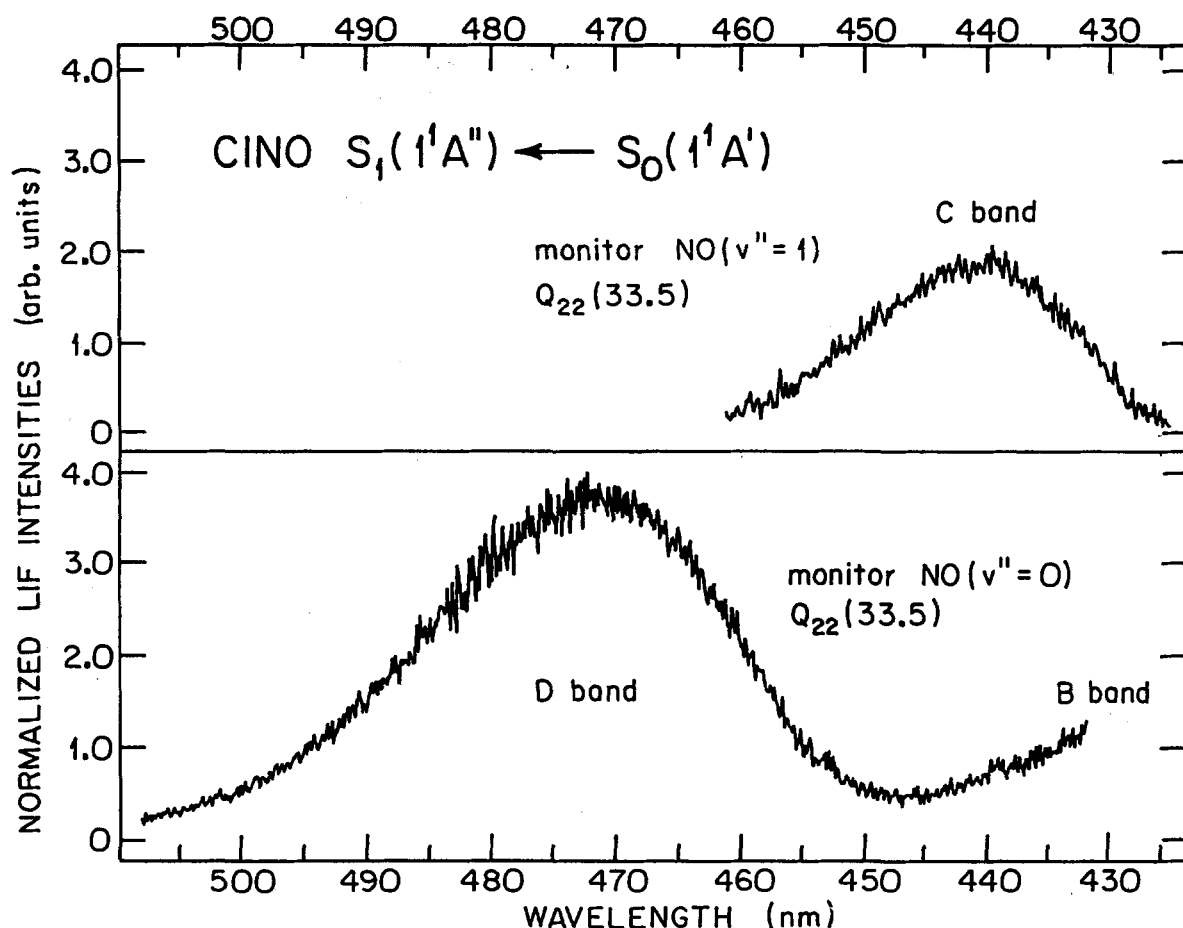
FIG. 1. PHOFRY spectra in the region of ClNO $S_1(1\ ^1A'') \leftarrow S_0(1\ ^1A')$ excitation. The upper panel obtained by monitoring NO($v'' = 1$) shows a peak corresponding to the C band in the absorption spectrum. This peak does not appear in the lower panel when NO($v'' = 0$) is monitored. The intensities of the bands are normalized to each other and reflect the relative partial absorption cross sections.

where S is the rotational line strength,[12] FC is the Franck–Condon factor for absorption,[13] I_{ph} is the photolysis laser intensity at 440 or 472 nm, and I_{pr} is the probe laser intensity when monitoring the $Q_{22}(33.5)$ lines of the (0–0) and (0–1) γ bands. The 0 and 1 subscripts denote $v'' = 0$ and 1, respectively. We assumed that the electronic oscillator strength is the same for the two transitions, and that the spin–orbit and Λ-doublet populations of $v'' = 0$ and 1 are similar (see below). In separate experiments, we found that the rotational distributions of $v'' = 0$ and 1 were similar, and did not vary significantly across the absorption band; therefore, detailed summations over all rotational levels were unnecessary. Also, when monitoring R_{22} and Q_{11} lines of NO($v'' = 0$), the same PHOFRY spectra were obtained as when monitoring Q_{22} lines. Thus, the spectra displayed in Fig. 1 indeed represent the relative absorption cross sections into S_1(000) and S_1(100). A comparison of the normalized peak heights at 472 and 440 nm yields ($v'' = 0/v'' = 1$) = 1.8 ± 0.2. Normalization of the peak heights by their respective widths yields the integrated partial cross section ratio [NO($v'' = 0$)] [NO)$v'' = 1$)] = 2.3 ± 0.4.

NO LIF spectra were obtained near the peaks of the D and C bands (467 and 440 nm, respectively), and rotational populations were derived for the two spin–orbit states of $v'' = 0$ and 1. As discussed before, the measured LIF line

intensities depend on the particular lasers detector geometry and polarization configuration, and have to be corrected for alignment effects.[5] Briefly, the line intensities are given by

$$I_{ie} = AS_{ie}N_i[b_0 + b_1\beta_0^2(02)], \qquad (2)$$

where I_{ie} is the intensity of a line originating from ground state level i to excited state e, S_{ie} is the rotational line strength, N_i is the population of level i, b_0 and b_1 are constants which are functions of J_i'', the rotational branch, and the specific lasers–detector configuration, and $\beta_0^2(02)$ is the bipolar moment describing rotational alignment.[14] $\beta_0^2(02)$ relates to the rotational alignment parameter $A_0^{(2)}$ by[14,15]

$$A_0^{(2)} = 0.8\beta_0^2(02). \qquad (3)$$

In our data processing, we compared two spectra obtained with the laser detector configurations described in Sec. II, one where $E_{ph}\|E_{pr}$ and a second where $E_{ph}\perp E_{pr}$ (referred to as geometries I and II, respectively, in Ref. 14), and we also took account of the spectral overlap between the branches. A least-squares fit program was used to normalize the two spectra using separate $\beta_0^2(02)$ constants for the $^2\Pi_{1/2}$ and $^2\Pi_{3/2}$ states. We assumed that $\beta_0^2(02)$ (and hence $A_0^{(2)}$) does not vary significantly with J'' for $J'' > 20.5$, as expected for high J''.[15] We found that the data from the two geometries were best normalized with $A_0^{(2)} = 0.64 \pm 0.10$
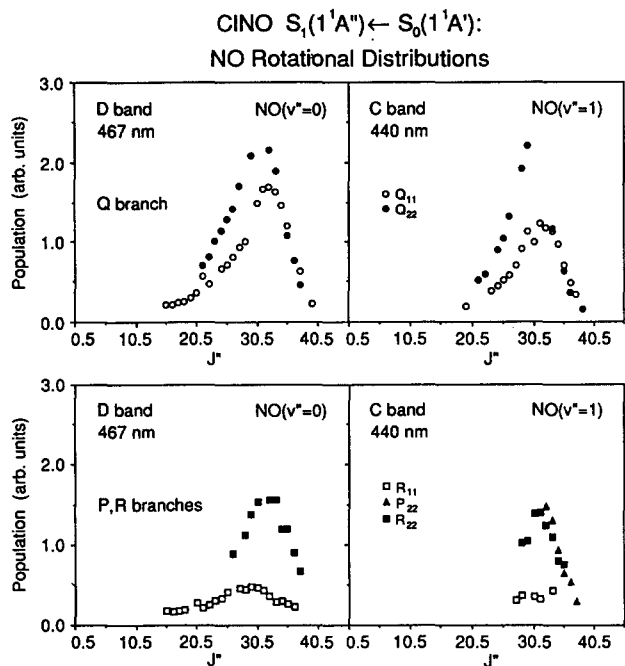
ClNO $S_1(1\,{}^1A'') \leftarrow S_0(1\,{}^1A')$:
NO Rotational Distributions

FIG. 2. NO $v'' = 0$ and 1 rotational populations obtained upon excitation of ClNO to $S_1(1\,{}^1A'')$. The 11 and 22 subscripts refer to lines originating in the ${}^2\Pi_{1/2}$ and ${}^2\Pi_{3/2}$ states of NO, respectively. **D** band excitation to $S_1(000)$ yields predominantly NO in $v'' = 0$, while **C** band excitation to $S_1(100)$ yields predominantly NO in $v'' = 1$. For each vibrational level, the relative scales of the upper and lower panels are identical, while the relative populations of $v'' = 0$ and 1 are not normalized. The conversion of line intensities to rotational populations is discussed in the text. The available energies with 467 and 440 nm excitations are 8413 and 7867 cm^{-1}, respectively.

and 0.68 ± 0.10 for NO in $v'' = 0$ and 1, respectively, in good agreement with previous results, [4,5] and the two spin–orbit states had similar alignment parameters. Since the limiting value of $A_0^{(2)}$ for a perpendicular transition is 0.8, our data show high degree of alignment. The rotational populations for NO $v'' = 0$ and 1 derived using Eq. (2) are plotted in Fig. 2. For each vibrational level, the relative scales of the upper and lower panels are identical, and the data are displayed separately only for convenience of viewing. The absolute peak heights of the $v'' = 0$ and 1 distributions do not reflect their relative populations. The rotational populations are inverted, peaking at $J'' \cong 30.5$, with nearly bell-shaped distributions and FWHM of $10 \pm 1\,J''$ for both vibrational levels. In addition, the ${}^2\Pi_{3/2}$ state (Q_{22}, R_{22}, and P_{22} lines) is more populated than the lower ${}^2\Pi_{1/2}$ state (Q_{11}, R_{11}, and P_{11} lines) for both vibrational levels. The $v'' = 0$ distribution obtained at 467 nm is similar to the corresponding distribution obtained at 499.4 nm, i.e., in the red wing of the **D** band.[5] The $v'' = 1$ distribution is similar to, but slightly narrower than the corresponding 470 nm NO($v'' = 1$) distribution obtained by Ticktin *et al.* with 300 K ClNO samples, using a single laser for photolysis and analysis and two-photon LIF detection of NO.[4] This wavelength lies in the red wing of the **C** band, and the larger width of the rotational distribution is probably due to the parent rotational excitation.

Several features are apparent in Fig. 2: (i) For NO $v'' = 0$ and 1, the ${}^2\Pi_{3/2}$ spin–orbit state is more populated than the ${}^2\Pi_{1/2}$ state. (ii) The NO(${}^2\Pi_{1/2}$) populations ob-

tained from Q branch lines are larger than those obtained by monitoring P or R branch lines for both $v'' = 0$ and 1. This indicates that the $\Pi(A'')$ Λ-doublet component is more populated than the $\Pi(A')$ component. We obtain for $J'' > 30.5$ the following average values for the Λ-doublet ratios: $\Pi(A'')/\Pi(A') = 3.4 \pm 0.4$ and 3.1 ± 0.4 for $v'' = 0$ and 1, respectively. (iii) The $\Pi(A'')$ preference is much smaller for ${}^2\Pi_{3/2}$, with an average $\Pi(A'')/\Pi(A') = 1.2 \pm 0.7$ for both $v'' = 0$ and 1. The Λ-doublet ratios are in good agreement with the values obtained by Bruno *et al.* for $v'' = 1$ with 300 K samples and 470 nm photolysis; $\Pi(A'')/\Pi(A') = 3.0$ and 1.4 for ${}^2\Pi_{1/2}$ and ${}^2\Pi_{3/2}$, respectively.[4]

In Fig. 3, we show for comparison the NO($v'' = 0$) rotational level distributions obtained with 440-nm photolysis (i.e., at the peak of the **C** band). According to Fig. 1, with this photolysis wavelength NO($v'' = 0$) derives from simultaneous dissociation on $S_1(000)$ and S_3, and indeed the previously measured vector properties, which are intermediate between the limiting values for parallel and perpendicular transitions, support this conclusion.[6] The rotational distributions are also in accord with this interpretation, as can be
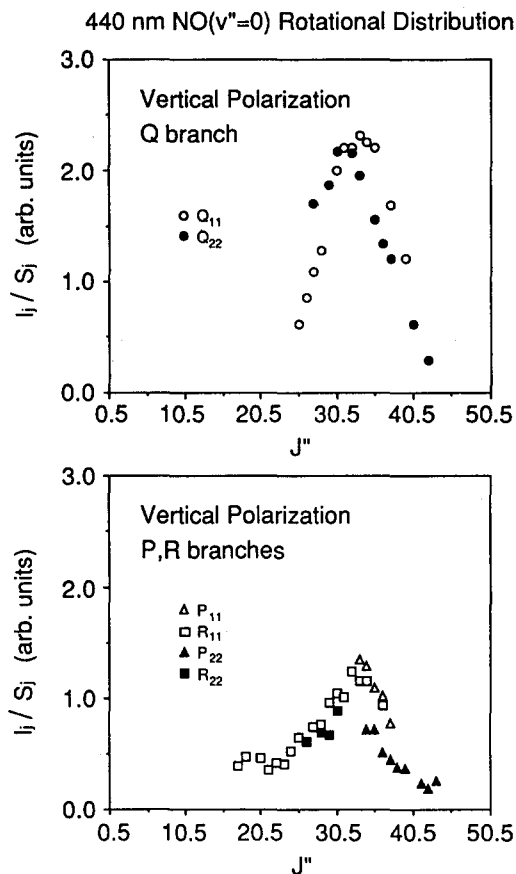
440 nm NO(v"=0) Rotational Distribution

FIG. 3. NO($v'' = 0$) rotational level distributions following excitation at 440 nm in the region between the **D** and **B** bands. The distributions are obtained from the LIF spectra by dividing the rotational line intensities I_j by the corresponding line strengths S_j. The level distributions were obtained with vertical photolysis laser polarization $E_{ph} \parallel E_{pr}$; E_{pr} is vertically aligned and k_{ph} is parallel to k_{pr} and horizontally aligned. At 440 nm, NO($v'' = 0$) derives from simultaneous dissociation on $S_1(000)$ and S_3, and the available energy is 9727 cm^{-1}.

seen from the following: (i) For pure S_3 excitation we observed $^2\Pi_{1/2} > {}^2\Pi_{3/2}$, while $^2\Pi_{1/2} < {}^2\Pi_{3/2}$ was obtained in dissociation on S_1;[6] with 440-nm photolysis, $^2\Pi_{1/2} \sim {}^2\Pi_{3/2}$. (ii) The Λ-doublet components with S_3 dissociation yield $\Pi(A'') > \Pi(A')$ for both spin–orbit states,[6] whereas with S_1 excitation, $\Pi(A'') > \Pi(A')$ for $^2\Pi_{1/2}$, while $\Pi(A'') \sim \Pi(A')$ for $^2\Pi_{3/2}$;[5,6] with 440 nm excitation, $\Pi(A'') > \Pi(A')$ even for $^2\Pi_{3/2}$. (iii) The S_3 surface is more repulsive than S_1, yielding larger torques and higher NO rotational excitation;[5,6] the rotational level distributions shown in Fig. 3 are broader and "hotter" than the corresponding S_1 distributions, again reflecting the mixed nature of the transition. Thus, the experimental evidence confirms the conclusion that at 440 nm, $NO(v'' = 1)$ derives exclusively from $S_1(100)$ excitation, while the much weaker $NO(v'' = 0)$ signal derives from mixed $S_1(000)$ and S_3 excitations. Note that different detection biases affect the NO rotational line intensities originating from S_1 and S_3 excitations (i.e., excitation via perpendicular and parallel transitions, respectively),[6] and therefore a conversion of level populations (i.e., LIF intensities divided by rotational line strengths) to rotational state populations was not attempted.

IV. DISCUSSION

A. Comparisons with theory

The experimental observations that can be directly compared with theory are the partial $S_1 \leftarrow S_0$ absorption cross sections into $S_1(000)$ and (100) (D and C bands, respectively), the width of the absorption bands, the NO vibrational populations as a function of the dissociation wavelength, and the $v'' = 0$ and 1 rotational distributions.

The spectroscopic assignments of the D and C bands to the $S_1 \leftarrow S_0$ transition yielding NO $v'' = 0$ and 1, respectively, appear now to be firm, being confirmed both by the experimental results and the quantum-mechanical calculations on a 3D PES.[10] The experimental ratio of the integrated partial absorption cross sections into $S_1(000)$ and $S_1(100)$ is 2.3 ± 0.4, while the calculated ratio obtained with $r_{NO} = 1.13$ Å (i.e., the optimized value in the FC region) is 3.42.[10] However, the uncertainty in the calculated r_{NO} is 0.02 Å, and a calculation using $r_{NO} = 1.12$ Å yields a ratio of 2.3, in good agreement with the experimental value.[10] On the other hand, in the calculations, the widths of the D and C bands are 1330 cm^{-1} FWHM for both bands, while the corresponding experimental values are 1300 ± 100 and 1000 ± 70 cm^{-1}. This will be more fully discussed in Sec. IV B. We note, however, that despite the existence of diffuse vibrational structure, the dissociation is fast and direct since the potential is repulsive in the Cl–N coordinate. Diffuse vibrational structure in direct dissociation processes has been observed in other molecules,[16,17] and treated theoretically using both time-dependent[18] and time-independent[19,20] formalisms, demonstrating that a diffuse vibrational structure can exist even when the dissociation time is shorter than a vibrational period.

The vibrational selectivity in the excitation is also well reproduced by theory; excitation in the D band yields predominantly NO in $v'' = 0$, while dissociation in the C band yields mainly $NO(v'' = 1)$.[10] The small $NO(v'' = 0)$ signal

observed in the C band region arises from simultaneous excitation in the blue wing of the D band and the red wing of the B band [i.e., on $S_1(000)$ and S_3]. It is noteworthy that only the state specific PHOFRY spectra can reveal the different contributions to the overlapping absorption features.

The inverted $NO(v'' = 0)$ rotational distribution is nicely reproduced by both quantal and classical calculations on the S_1 PES; like the experimental distribution, the calculated distribution is bell-shaped, and peaks at $J'' = 30.5$ with FWHM of $11 J''$.[10] A more detailed comparison is difficult, because the calculations do not take into account the Λ-doublet and spin–orbit propensities. Thus, for quantitative comparisons, a summation over all the rotational branches and both spin–orbit states is necessary. However, this is difficult because of spectral overlaps of rotational lines in several branches. A comparison between the rotational distribution derived from $v'' = 0$ Q_{22} branch lines and the calculated distribution shows very good agreement (e.g., compare Fig. 2 of the present paper with Fig. 4 of Ref. 10).

In general, the widths and shapes of fragment rotational distributions obtained with jet-cooled samples are determined by one or more of the following:[10] (i) the shape of the bending wave function in the ground electronic state, or in the case of slower dissociation, in the excited state;[8] (ii) the impulsive torque induced by photon absorption; and (iii) the angular anisotropy in the excited-state PES along the reaction coordinate. According to the calculations on the S_1 PES of ClNO,[10] the rotational distribution is determined mainly by the impulsive force along the Cl–N bond that causes closing of the angle during the bond separation, and the anisotropy in the exit channel angular potential which has a counteracting effect in inhibiting free rotation. The overall rotational excitation is therefore smaller than predicted by the impulsive model.[10] The calculations also show that the width of the parent vibrational wave function on the ground electronic state is not directly reflected in the width of the rotational distribution, which is narrower as a result of the torques acting along the reaction coordinate.[10] In other words, the original wave packet prepared in the FC region subsequently propagates under the influence of the forces on the S_1 PES. The motion of the wave packet can be divided into two parts: the center of the wave packet follows a classical trajectory, thereby developing angular momentum, while the size of the wave packet may also change in the angular coordinate during the dissociation. As per the uncertainty principle, an increase in size of the wave packet is accompanied by a decrease in the momentum spread, giving rise to a narrower final rotational distribution. The broadening of the wave packet is in agreement with the wave function description shown in Fig. 9 of Ref. 10.

B. Dissociation dynamics on S_1

By combining the experimental and theoretical results, the following picture of the photodissociation dynamics on S_1 emerges. Upon photon absorption in the FC region, dissociation commences as a result of the repulsion between Cl and NO. Although in general the potential along the Cl–N coordinate is repulsive and the dissociation is fast and direct,

a diffuse structure in the NO stretch coordinate of the upper state persists.

We suggest that the narrower width of the $S_1(100) \leftarrow S_0$ band compared with the $S_1(000) \leftarrow S_0$ band results from the differences between the parent NO stretch frequency in $S_1(1500 \text{ cm}^{-1})$ and in free NO(1860 cm^{-1}). Assuming an adiabatic evolution of parent NO stretch excitation into NO vibration, the optimized potential curves along the reaction coordinate are separated by 1500 cm^{-1} near the FC region, and 1860 cm^{-1} in the asymptotic region. Consequently, the PES associated with NO($v'' = 1$) is less steep than the one associated with NO($v'' = 0$) giving rise to slightly slower dissociation. Alternatively, using a time-dependent wave packet representation, the flatter curve should allow more recurrences in the autocorrelation function, and therefore lead to a narrower bandwidth. A narrowing of the band-width with increasing parent NO stretch excitation in the excited state has also been observed in dissociation of ClNO on T_1^8 and HONO on S_1,[16(b)] and in both molecules the parent NO stretch frequency is smaller than the free NO vibrational frequency. The lifetimes derived from the observed bandwidths, 4.1 ± 0.3 and 5.3 ± 0.4 fs for the **D** and **C** bands, respectively, do not represent the dissociation times, but rather the propagation times of the wave packets out of the FC region.[18]

Using the measured widths of the **D** and **C** bands, we can roughly estimate the range of the $R-r$ interaction (where R is the distance between Cl and the center of mass (c.m.) of NO, and r is the internuclear separation in NO) from the calculated slopes of the PES in the R coordinate near the FC region. To achieve that, a pseudodiatomic picture of the potential curve along the dissociating bond is adopted, as described by Herzberg.[21] In this picture, the normal modes in the ground state are assumed to be separable, so that only the Cl-N stretch wave function is "reflected" into the repulsive surface along the R coordinate.[9,21,22] We also assume that the excited-state NO stretch vibrations evolve adiabatically into NO vibrations. The slope of the repulsive potential curve along the R coordinate near the FC region, $dV/dR\,|_{R_{e''}}$ can be obtained from the measured absorption linewidth and the ground-state vibrational wave function, assuming that the slope depends linearly on R near $R_{e''}$. As described by Herzberg, the absorption cross section $\sigma(E)$ is proportional to the square of the ground-state vibrational wave function in the R coordinate:[21]

$$\sigma(E) \propto \nu |\Psi_R''(E)|^2, \quad (4)$$

where ν is the frequency of the absorbed photon, and $\Psi_R''(E)$ is given in terms of the excitation energy E:

$$\Psi_R''(E) = k\{\exp[-\alpha(E - E_0)^2/2]\}, \quad (5)$$

where E_0 is the excitation energy at the center of the absorption band, k is a constant, $\alpha = \alpha_R/|dV/dR\,|_{R_{e''}}$, and $\alpha_R = 2\pi\omega_R''\mu/h$ is the harmonic oscillator constant.[21] dV/dR is related to the bandwidth of the absorption band ΔE by $|dV/dR\,|_{R_{e''}} = -\Delta E/\Delta R$ where ΔR is the FWHM of the ground-state wave function in the R coordinate. By using the spectroscopic values of ω_R'',[23,24] and the measured bandwidths in the PHOFRY spectra for $v'' = 0$ and 1, we obtain $S = -1.64$ and -1.27 eV/Å for $v'' = 0$ and 1, respectively
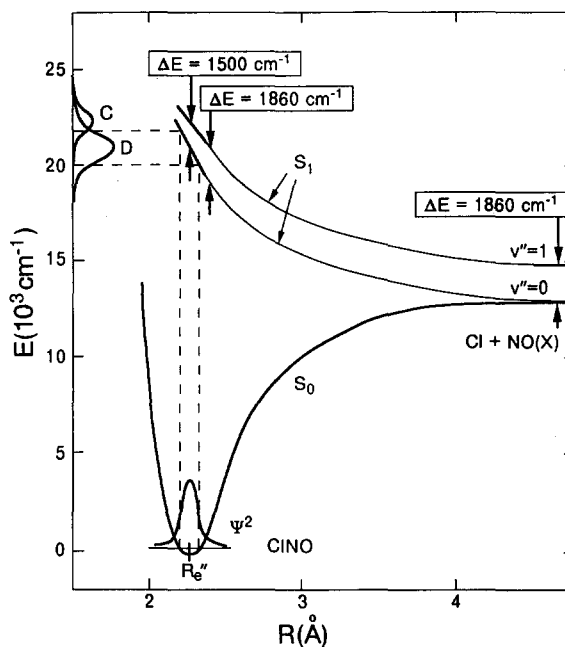

FIG. 4. Pictorial representations of cuts in the potential surfaces in the R coordinate near the FC region. R is the distance between the Cl atom and NO c.m. The two curves correspond to excitations in $S_1(000)$ and $S_1(100)$ that evolve asymptotically to NO $v'' = 0$ and 1, respectively. The slopes in the FC region are calculated by the "reflection principle" from the measured widths of the **D** and **C** absorption bands, shown schematically on the left.

(**D** and **C** bands). By using these gradients and assuming linearity of the potential curves in the FC region, we find that the difference between the curves changes from 1500 to 1860 cm^{-1} when R increases from $R_{e''}$ to $R_{e''} + 0.12\text{Å}$. This distance is comparable to the FWHM of the square of the ground-state wave function, $\Delta R = 0.098\text{Å}$ FWHM.[21,22] Thus, the slopes are different mainly in the FC region, and it is there that most of the $R-r$ interaction probably takes place.[24] Beyond this region, the energy difference between the curves correlating with $v'' = 0$ and 1 is constant and equal to the asymptotic value of the NO vibrational frequency. A pictorial representation of the relevant cuts in the PES, as deduced from the observed bandwidths of the **D** and **C** bands, is shown in Fig. 4. The thick solid lines near the FC region indicate the region where the slopes of the curves yielding asymptotically NO $v'' = 0$ and 1 are different.

It appears, therefore, that the NO vibrational distribution is established early, following the initial couplings between the R and r coordinates, and the evolution of parent NO excitation into free NO vibration is largely adiabatic. This justifies the separate treatment by the theory of the rotational and vibrational excitations.[10] We also observe that despite the differences in the steepness of the $S_1(000)$ and $S_1(100)$ potential curves near the FC region, the NO rotational distributions in $v'' = 0$ and 1 are similar. This is not surprising, since the calculations indicate that the final rotational distributions are determined at larger Cl–N distances, where the anisotropy in the angular potential modifies the initial angular momentum induced by the impulsive force.[10] In other words, final-state interactions influence the rotational distributions at larger internuclear separations along

the R coordinate, after the vibrational distribution has already been fixed. Thus, the overall picture favors independent evolution of vibrational and rotational excitation, subsequent to the initial couplings between the R and r coordinates near the FC region.

The vector properties also agree with the fast and direct nature of the photodissociation, and both the recoil anisotropy and the rotational alignment parameters are close to their limiting values. An intriguing observation concerns the Λ-doublet components in NO($X\,^2\Pi$). We find that for the $^2\Pi_{1/2}$ state, the $\Pi(A'')$ Λ-doublet component[25] is significantly more populated than the $\Pi(A')$ component both for $v'' = 0$ and 1. This propensity reflects the orientation of the singly occupied molecular orbital in S_1, which is of a'' symmetry. It indicates that despite the existence of strong final-state interactions in the exit channel (as manifested in the large NO rotational excitation), the initial orientation of the excited NO π^* lobe in ClNO is largely preserved in the dissociation.[6] In contrast, the Λ-doublet preference in the $^2\Pi_{3/2}$ state is much smaller. Although we presently do not have a model for explaining the greater loss of Λ-doublet preference in the $^2\Pi_{3/2}$ state, the loss of orientation of the NO π^* lobe may derive from state-specific perturbations with other surfaces. For example, our *ab initio* calculations show that the $T_2(1\,^3A')$ surface crosses the S_1 surface near the FC region and also at larger Cl–N separations.[6] The calculations also show that T_2 has a singly occupied molecular orbital of a' symmetry, which upon dissociation should show a propensity for the $\Pi(A')$ NO Λ-doublet component. Therefore, perturbations by T_2 may cause a decrease in the $\Pi(A'')$ preference of NO ($^2\Pi_{3/2}$) on S_1. The photodissociation dynamics, though, appears to take place on the S_1 PES, and the rotational and vibrational distributions are not affected by the proximity of T_2.

An unexplained observation concerns the NO spin–orbit population ratios, which favor the upper spin–orbit state. We believe that the spin–orbit populations are established later in the exit channel, after nuclear motions such as NO rotations have developed. However, it is hard to predict the spin–orbit population ratios in NO, since they may be the result of numerous couplings and uncouplings between the surfaces as the NO spin–orbit states establish their separate identities. The population of the spin–orbit states of Cl ($^2P_{1/2}$ and $^2P_{3/2}$) could not be determined with the present resolution of our sub-Doppler experiments.[5]

C. Comparisons between dissociations on S_1 and T_1

Both S_1 and T_1 derive from excitation of a predominantly nonbonding electron centered on Cl and O to an out-of-plane π^* orbital centered on NO.[6] Thus, the two excited states have the same molecular orbital configuration, except for spin, and a comparison between the photodissocition dynamics on the two surfaces is insightful. Dissociation on T_1 has been recently studied in detail and the major findings are:[6–8] (i) The absorption and PHOFRY spectra show diffuse structure both in the bending and the NO stretch coordinates. The widths of the peaks increase with increasing number of bending quanta, but decrease with increasing ν_1 excitation, and are in the range 100–330 cm^{-1}. (ii) Parent

NO stretch excitation evolves adiabatically into free NO vibrational excitation. (iii) Parent bending excitation evolves into NO rotations, and the rotational distributions depend on the number of bending quanta. The fraction of energy in NO rotation, however, is rather small in all cases, and the main source of NO angular momentum is the ClNO parent bending wave function. Only a modest torque is generated by the angular anisotropy in the T_1 PES, and all the rotational distributions peak near $J'' = 0.5$.

The relatively narrow absorption features in the $T_1 \leftarrow S_0$ transition, and the low rotational excitation of NO from dissociation on T_1 suggest that the T_1 surface is less impulsive along the Cl–N bond, and more isotropic along the reaction coordinate than the S_1 surface. This is partly due to the lower excess energies involved in the dissociation on T_1 and S_1, ~ 3000 vs 8200 cm^{-1}, respectively. However, had the impulse in T_1 been directed along the Cl–N bond, higher rotational excitation would have been obtained according to the impulsive model,[26] i.e., $E_{\text{rot}} = 1073$ cm^{-1}, as compared with the measured values of 90–340 cm^{-1}.[8] In other words, the impulsive force on T_1 is directed away from the Cl–N bond and towards the NO center of mass, while on S_1 its direction is mainly along the Cl–N bond.

The repulsion along the Cl–N bond is related to the electron distribution in the excited state. Inspection of the total atomic charge distributions in the excited states shows that upon excitation to T_1, electronic charge is removed from Cl and transferred to NO, whereas no net charge transfer occurs on S_1.[6] The relevant charge distributions on Cl, N, and O for T_1 are $+0.556$, -0.310, and -0.246, respectively, while the corresponding charges on S_1 are -0.041, $+0.061$, and -0.020.[6] On T_1, the charge-transfer excitation tends to delocalize the electron density in the molecule, and the opposite charges on Cl and NO tend to decrease the repulsion. On the other hand, on S_1, Cl and NO have a predominantly free radical structure, similar to the free species, and more electron density is concentrated in the region of the Cl–N bond. Since excitation involves promotion of an electron to an antibonding orbital, the two electrons arranged in the singlet configuration (opposite spins) experience more repulsion than in the triplet configuration, where the spins are parallel. This conclusion is also supported by inspection of the Mulliken coefficients of the atomic orbitals in S_1 and T_1, which exhibit the same trends as the total charge distributions.[27] Thus, dissociation on S_1 is expected to be faster and more impulsive along the Cl–N coordinate than on T_1, resulting in broader bandwidths and larger rotational excitations.

An important difference between the dissociations on S_1 and T_1 involves the origins of the NO rotational angular momentum. On T_1, which dissociates more slowly, the identity of the bending wave function is well established before dissociation, as evidenced by the existence of several bending progressions in the absorption spectrum.[8,9] Thus, the rotational excitation is influenced by the shape of the bending wave functions *in the excited state* and reflects their associated nodes. Since the impulsive torque on T_1 is much smaller than on S_1, the main contributions to the (weak) NO rotational excitations come from the angular momentum inher-

ent in the T_1 bending wave functions, and the modest angular anisotropy in the exit channel. In contrast, the faster dissociation on S_1 does not allow the development of separate bending wave functions in the excited state, and it is the ground-state bending wave function that propagates on S_1. As was shown by Schinke et al.,[10] the main sources of angular momentum in this case are the large impulsive force along the Cl–N bond, and the counteracting force due to the angular anisotropy in the potential. Thus, NO rotational excitation from dissociation on S_1 is much larger than on T_1, and the fast dissociation process can be treated by classical mechanics.[10]

Although the NO rotational distributions generated in the dissociation on T_1 and S_1 are different, the origins of NO vibrational excitation on the two surfaces are similar. As on S_1, the free NO vibrational excitation following dissociation on T_1 is established quite early, and following the initial coupling of the NO stretch coordinate to the other coordinates, the evolution of parent NO stretch to NO vibration is largely adiabatic. Thus, on both surfaces, the evolution of the rotational and vibrational excitations appear to be uncoupled, and can be treated separately.[8,10]

V. SUMMARY

(1) The dissociative $S_1(1\,^1A\,'') \leftarrow S_0(1\,^1A\,')$ perpendicular transition shows diffuse vibrational structure with a progression in ν_1, the NO stretch mode. The absorption and PHOFRY spectra consist of two bands, corresponding to excitations in $S_1(000)$ and $S_1(100)$, respectively. The relative partial absorption cross sections are $S_1(000):S_1(100) = 2.3:1.0$, in good agreement with the ratios obtained by dynamical calculations on a 3D PES calculated ab initio.[10] The widths of the $S_1(000)$ and $S_1(100)$ bands are 1300 ± 100 and 1000 ± 70 cm^{-1}, respectively. The narrowing of the absorption bands with increasing ν_1 quanta results from the mismatch between ν_1 and the free NO vibrational frequency.

(2) Despite the existence of vibrational structure in the absorption spectra, the dissociation is fast and direct. Parent NO stretch excitation evolves adiabatically into NO vibrational excitation; dissociations on $S_1(000)$ and $S_1(100)$ yield NO $v'' = 0$ and 1, respectively. The NO($X\,^2\Pi$) rotational distributions in $v'' = 0$ and 1 are inverted, peaking at $J'' \sim 30.5$ with a width of $10 \pm 1\,J''$, in good agreement with classical and quantum-mechanical calculations.[10] The rotational distributions do not vary significantly when the photolysis laser is scanned across the absorption bands. The evolution of NO vibrational and rotational excitations appear to be largely uncoupled. The vibrational distribution is determined near the FC region, while final-state interactions affect the rotational distributions at larger Cl–NO separations.

(3) In NO $v'' = 0$ and 1, the upper spin–orbit state $^2\Pi_{3/2}$ is more populated than the lower state, $^2\Pi_{1/2}$, but the relative populations of Cl $^2P_{1/2}$ and $^2P_{3/2}$ are unknown. The Λ-doublet $\Pi(A\,'')$ component of NO($^2\Pi_{1/2}$) is more populated than the $\Pi(A\,')$ component by a ratio of $\sim 3:1$, as expected for excitation to a π^* orbital of a'' symmetry, but this propensity is much lower for NO($^2\Pi_{3/2}$), possibly because of perturba-

tions by the nearby T_2 state.

(4) Comparisons with dissociation on T_1 show that the evolution of vibrational excitation is similar on the two surfaces, while the NO rotational distributions are strikingly different, probably as a result of the differences in the dissociation rates and the charge distributions in the two excited states.

[1] G. E. Busch and K. R. Wilson, J. Chem. Phys. **56**, 3655 (1972).

[2] (a) M. D. Moser, E. Weitz, and G. C. Schatz, J. Chem. Phys. **78**, 757 (1983); (b) M. D. Moser and E. Weitz, Chem. Phys. Lett. **82**, 285 (1981).

[3] D. Solgadi, F. Lahmani, C. Lardeux, and J. P. Flament, Chem. Phys. **79**, 225 (1983).

[4] (a) A. E. Bruno, U. Brühlmann, and J. R. Huber, Chem. Phys. **122**, 155 (1988); (b) A. Ticktin, A. E. Bruno, U. Brühlmann, and J. R. Huber, *ibid.* **125**, 403 (1988).

[5] A. Ogai, C. X. W. Qian, L. Iwata, and H. Reisler, Chem. Phys. Lett. **146**, 367 (1988).

[6] Y. Y. Bai, A. Ogai, C. X. W. Qian, L. Iwata, G. A. Segal, and H. Reisler, J. Chem. Phys. **90**, 3903 (1989).

[7] C. X. W. Qian, A. Ogai, L. Iwata, and H. Reisler, J. Chem. Phys. **89**, 6547 (1988).

[8] C. X. W. Qian, A. Ogai, L. Iwata, and H. Reisler, J. Chem. Phys. **92**, 4296 (1990).

[9] C. F. Goodeve and S. Katz, Proc. R. Soc. London Ser. A **172**, 432 (1939).

[10] R. Schinke, M. Nonella, H. Suter, and J. R. Huber, J. Chem. Phys. **93**, 1098 (1990).

[11] *JANAF Thermochemical Tables*, 2nd ed., edited by D. R. Stull and H. Prophet, Natl. Stand. Ref. Data Ser., Natl. Bur. Stand. No. 9 (National Bureau of Standards, Washington, D. C., 1967).

[12] L. T. Earls, Phys. Rev. **48**, 423 (1935).

[13] S. N. Suchard, Aerospace Report No. TR-0074(464)-6 (1974), Vol. II.

[14] R. N. Dixon, J. Chem. Phys. **85**, 1866 (1986).

[15] C. H. Greene and R. N. Zare, J. Chem. Phys. **78**, 6741 (1983).

[16] (a) G. W. King and D. Moule, Can. J. Chem. **40**, 2057 (1962); (b) J. H. Shan, S. J. Wategaonkar, and R. Vasudev, Chem. Phys. Lett. **158**, 317 (1989).

[17] P. Tarte, J. Chem. Phys. **20**, 1570 (1952).

[18] (a) E. J. Heller, J. Chem. Phys. **68**, 2066 (1978); (b) **68**, 3891 (1978); (c) Acc. Chem. Res. **14**, 368 (1981).

[19] R. Pack, J. Chem. Phys. **65**, 4765 (1976).

[20] R. Schinke, S. Hennig, A. Untch, M. Nonella, and J. R. Huber, J. Chem. Phys. **91**, 2016 (1989).

[21] (a) G. Herzberg, *Spectra of Diatomic Molecules* (Van Nostrand, New York, 1950); (b) *Spectra of Polyatomic Molecules* (Van Nostrand, New York, 1966).

[22] R. Schinke, in *Collision Theory for Atoms and Molecules*, edited by F. A. Gianturco, (Plenum, New York, 1989).

[23] (a) L. H. Jones, R. R. Ryan, and L. B. Asprey, J. Chem. Phys. **49**, 581 (1968); (b) J. K. McDonald, J. A. Merrit, V. F. Kalasinsky, H. F. Heusel, and J. R. During, J. Mol. Spectrosc. **117**, 69 (1986).

[24] In the calculations we have used the frequency $\nu_2'' = 595.8$ cm^{-1}; however, the normal modes in ClNO are of a mixed nature. If we use, instead, $\nu_3'' = 331.9$ cm^{-1}, which also has a large Cl–N stretch character (Ref.

23), we get $S = -1.22$ and -0.94 eV/Å for the **D** and **C** bands, respectively. However, we still find that the two curves become parallel near the FC region, since $R = R''_e + 0.16$Å, which is comparable to the FWHM of the square of the ground-state wave function, $\Delta R = 0.13$Å. We note that the separation of the ground-state wave function into independent stretch and bend modes is not justified in CINO, because of the large coupling between the Cl–N stretch and bend modes, and we use the separated func-

tions here only to qualitatively demonstrate our point.

[25] (a) P. Andresen and E. W. Rothe, J. Chem. Phys. **82**, 3634 (1985); (b) M. H. Alexander and P. J. Dagdigian, *ibid.* **80**, 4863 (1984); (c) M. H. Alexander *et al.* (29 authors), *ibid.* **89**, 1749 (1988).

[26] (a) A. F. Tuck, J. Chem. Soc. Faraday Trans. 2 **73**, 689 (1977); (b) R. Schinke, Comments At. Mol. Phys. **23**, 15 (1989).

[27] Y. Y. Bai (unpublished).